

# Modeling and Control of a Kite on a Variable Length Flexible Inelastic Tether

Paul Williams,\* Bas Lansdorp, Wubbo Ockels  
*Delft University, The Netherlands*

**This paper deals with the modeling of a tethered kite system. Such systems have the potential to generate power by driving a ground generator from winds at high altitude. To test the validity of controllers developed for the system, it is necessary to employ models of various sophistication. In this paper, the tether is modeled as a collection of point masses connected by inelastic rods. A simple procedure for efficiently determining the tension constraint forces is developed. The procedure used for deploying and retrieving the cable in the model is also presented. This entails the addition and subtraction of elements in the model. A simple feedback controller is derived to maneuver the kite in the cross-wind direction and for maintaining the tether tension at the desired level. The tether length is controlled to maintain the desired altitude of the kite. Numerical results demonstrate the effectiveness of the controller and efficiency of the tether model.**

## I. Introduction

**W**IND energy is an important resource that can be potentially exploited in new renewable energy systems. Over the last several decades, many proposals have been put forward for devices to extract and utilize wind energy. The most popular design is based on the wind turbines placed relatively close to the ground. However, it has long been known that the Earth's surface creates a boundary-layer-like effect on the wind so that the wind speed generally increases with altitude. In fact, it is possible for significant wind to be present at higher altitudes with little to no wind on the ground. This knowledge has spawned several radical ideas for wind power extraction. However, many of the basic principles of transmitting wind energy to the ground have been used since the early days of kite-flying, when kites were used for towing boats and wagons,<sup>1</sup> or for lifting objects such as weather instrumentation.<sup>2</sup> In these applications, a kite is flown so as to produce a beneficial lifting or pulling force that is transmitted to an object at lower altitude via a tether. However, as pointed out by Carpenter,<sup>1,2</sup> with the advent of manned aircraft, such devices are seldom used today. One of the major problems encountered in early application of kites for towing vehicles was the lack of adequate feedback control to cope with changing and unsteady winds. Modern day control techniques are capable of circumventing some of these problems, which has seen renewed interest in kite research.<sup>1-</sup>

35

One of the most promising applications of tethered kites is for providing a means of generating electricity. By controlling the forces on the kite, thereby influencing the cable tension, it is possible to generate net power by utilizing a drum that is capable of paying the cable in- and out. If the tether is let out at high tension, it is generating power. If the tether is then reeled back in, it is using power. The key idea is to control the kite in such a way that the tension during the reel-in phase is much lower than the tension during the pay-out phase. The larger the difference in tension during reel-in and reel-out, the greater the power that can be generated. At the most basic level, if control of the kite motion can be achieved remotely, then it is possible to manipulate the tension in the tether by changing the forces on the kite. For example, to increase tension, the kite angle of attack can be increased, thereby increasing the lift on the kite. Conversely, to decrease tension, the kite angle of attack is decreased. Much more complex motions can be envisaged. The forces on the kite are a function of the kite angle of attack, its roll angle, and the local relative air speed. The most important of these for increasing the total lift force is the air speed, since doubling it results in a four-fold increase in lift. Therefore, ways of achieving higher relative air speeds is an important issue to be addressed.

In studies of kite systems for wind energy generation, the tether has been modeled under the assumption that it remains perfectly straight. In Ref. 33, the tether was modeled as an inelastic rod with distributed mass and drag. It is also relatively easy to consider the effects of longitudinal elasticity by modeling the tether as a single extensible

---

\* AIAA Member, e-mail: tethered.systems@gmail.com.

spring. For controller design/testing, it is preferable to develop a model that provides high accuracy of the simulated system with low computational burden. Typically, tether models of differing degrees of accuracy can be used. A natural approach is to represent the tether as a continuum, which entails the use of partial differential equations. A choice must be made as to whether the cable is treated as elastic or inelastic. Continuum models must be discretized for implementation, either via finite differences or by an assumed modes approach. Alternatively, physically discretized models have become prominent in the literature of towed and tethered systems due to their ease of implementation combined with good accuracy. In this paper, a highly efficient tether model, originally developed in Ref. 36 for trajectory optimization of tethered satellites, is presented for modeling a kite attached to a tether with a fixed base. The model incorporates all forces acting on the system except for the effects of tether elasticity.

This paper develops a simulation model and preliminary feedback control algorithm for controlling the kite position. The control variables for the kite are assumed to be the kite angle of attack and roll angle. Together these controls specify the resultant lift/drag forces on the kite under the assumption that its aerodynamic characteristics are known. The kite is connected to a tether, which is modeled based on a lumped mass approach.

## II. Dynamic Modeling of Tethered Kite System

The most basic kite system consists of a ground based generator and winch (drum), a tether, and a kite. In this paper, the main focus is on modeling the tether dynamics for the variable length case. In previous work on the kite system, various models have been used, including a lumped mass tether model in Ref. 32. However, the simulations performed in Ref. 32 were for two-dimensional motion only. The rationale for developing an efficient model is so that it can be used for preliminary control design. A great deal of research has been performed on tether modeling in a variety of environments. This paper draws on this research to develop an efficient tether model based on the lumped mass approach.

In the lumped mass approach, the tether is physically divided into a series of point masses connected by either elastic or inelastic links. The mass of the tether is “lumped” to the discrete masses, together with any external forces acting on the tether. The advantage of this formulation is that it is very intuitive and easy to include a variety of forces on the system. The approach has been validated using both comparisons with more sophisticated continuum approaches as well as with experimental results. When the links are elastic, the internal tether tension is determined as an explicit function of the lumped mass positions. For example, Hooke’s law can be used, which models the tension as a linear function of strain. In the lumped mass approach, the strain is assumed to be uniform within each element, but can vary over the length of the tether. Another advantage of modeling the tether as elastic is that the equations of motion are inertially decoupled. This means that the computation of state derivatives for integration is very efficient. On the other hand, the major drawback with modeling the tether as elastic, particularly when the tether has a high stiffness, is that small integration steps must be used to capture the high frequency vibrations. Alternatively, stiff integrators may be required, which can also result in long simulation times if the Jacobians needed by the integrator are calculated via numerical differentiation.

The tether is modeled using inelastic links in this work. The advantage of this approach is that the high frequency longitudinal oscillations are removed from the analysis. In general, this results in dramatic reductions in simulation time due to the removal of high frequency content from the cable dynamics. The geometric shortening of the distance to the tether tip is accounted for due to the changes in geometry of the system, but stretching of the tether is not. The degree of approximation is controlled by the number of discretized elements that are used.

There are three different approaches that can be used to generate the same physical model, but with different implications in terms of complexity and numerical cost. The first is to employ generalized mechanics principles, such as Lagrange’s equations or Kane’s equations. These approaches require that a minimum number of coordinates be used to represent the system. The result is generally a large set of complex equations that are coupled inertially, i.e., a mass matrix  $2N \times 2N$  would need to be inverted, where  $N$  is the number of elements. A second approach that can be used is to derive the equations of motion directly via Newton’s second law in Cartesian coordinates. To determine the unknown tension forces, a set of constraint equations (usually stabilized) are added to the system. The dynamic equations and constraint equations are then solved simultaneously for the system accelerations and tension forces. The approach that is adopted in this paper is similar to the second approach, except that the constraint equations are derived directly from the equations of motion by first applying a coordinate transformation to the dynamic equations. This effectively breaks up the pendulum motion of each mass from the longitudinal dynamics of each element, which enables the determination of the internal tension forces in a very efficient manner. The tension forces are essentially constraint forces that maintain the tether links at the correct lengths.

The system model is represented as shown in Fig. 1. An inertial coordinate frame is attached at the exit of the tether winch at  $O$ . The inertial axes are defined such that the  $x$ -axis points in the direction of the nominal wind, the  $z$ -

axis points vertically upward, and the  $y$ -axis completes the right-handed triad. The tether is modeled as consisting of a series of  $n$  point masses connected via inelastic links. The numbering is such that the kite is mass 1 and the last deployed element is  $n$ . This numbering is only for convenience when considering deployment and retrieval of the tether and its algorithmic implementation.

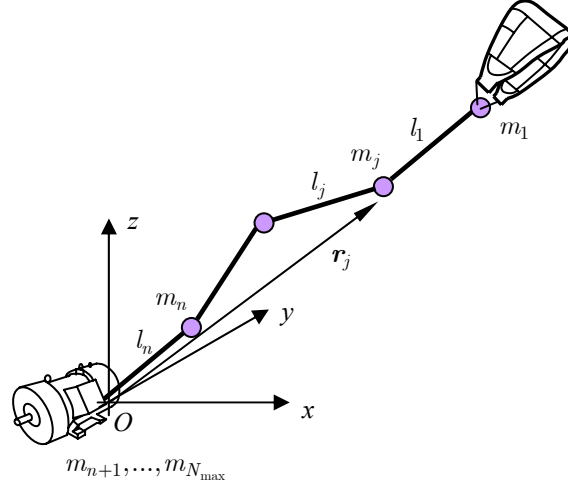


**Fig. 1 Kite system modeled with a flexible tether.**

The distribution of mass in the system is approximated via

$$m_j = \begin{cases} m_{\text{kite}} + \frac{1}{2} \rho_c A_1 l_1, & j = 1 \\ \frac{1}{2} \rho_c (A_j l_j + A_{j-1} l_{j-1}), & j = 2, \dots, n \end{cases} \quad (1)$$

where  $\rho_c$  is the cable mass density,  $A_j$  is the cross-sectional area of the  $j$ th element, and  $l_j$  is the length of the  $j$ th element. Consider the  $j$ th lumped mass,  $m_j$ . The position vector in the inertial coordinate system is denoted by  $\mathbf{R}_j$ . The equations of motion for the  $j$ th mass are obtained in a straightforward manner

$$m_j \ddot{\mathbf{R}}_j = \mathbf{F}_j \quad (2)$$

Clearly, this is the simplest form of the equations if Cartesian coordinates are used to represent the positions. However, Cartesian coordinates complicate the determination of the tension constraint forces and so we seek an alternative representation. Let the position of the  $j$ th mass relative to the  $(j+1)$ th mass be written as

$$\mathbf{r}_j = \mathbf{R}_j - \mathbf{R}_{j+1} \triangleq [l_j \cos \phi_j \sin \theta_j, l_j \sin \phi_j, l_j \cos \phi_j \cos \theta_j]^T \quad (3)$$

where  $l_j$  is the length of the  $j$ th segment,  $\theta_j$  is the angle of the segment to the vertical, and  $\phi_j$  is the out-of-plane angle of the segment.

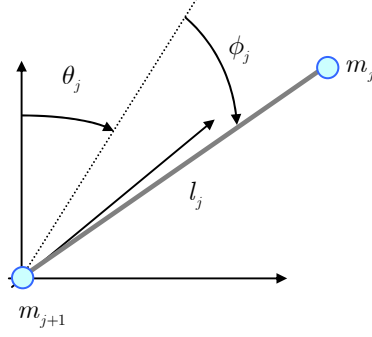


**Fig. 2 Spherical coordinates used to represent the orientation of the  $j$ th cable element.**

If Eq. (3) is differentiated twice with respect to time, and utilizing Eq. (2) we have that

$$\ddot{\mathbf{r}}_j = \frac{\mathbf{F}_j}{m_j} - \frac{\mathbf{F}_{j+1}}{m_{j+1}} \quad (4)$$

The components of the local relative velocity and acceleration are given by

$$\dot{\mathbf{r}}_j = [\dot{l}_j \cos \phi_j \sin \theta_j - l_j \dot{\phi}_j \sin \phi_j \sin \theta_j + l_j \dot{\theta}_j \cos \phi_j \cos \theta_j, \dot{l}_j \sin \phi_j + l_j \dot{\phi}_j \cos \phi_j, \dot{l}_j \cos \phi_j \cos \theta_j - l_j \dot{\phi}_j \sin \phi_j \cos \theta_j - l_j \dot{\theta}_j \cos \phi_j \sin \theta_j] \quad (5)$$

$$\begin{aligned} \ddot{\mathbf{r}}_j = & [\ddot{l}_j \cos \phi_j \sin \theta_j - 2\dot{l}_j \dot{\phi}_j \sin \phi_j \sin \theta_j + 2\dot{l}_j \dot{\theta}_j \cos \phi_j \cos \theta_j - l_j \dot{\phi}_j^2 \cos \phi_j \sin \theta_j \\ & - l_j \ddot{\phi}_j \sin \phi_j \sin \theta_j - 2l_j \dot{\phi}_j \dot{\theta}_j \sin \phi_j \cos \theta_j - l_j \dot{\theta}_j^2 \cos \phi_j \sin \theta_j + l_j \ddot{\theta}_j \cos \phi_j \cos \theta_j, \\ & \ddot{l}_j \sin \phi_j + 2\dot{l}_j \dot{\phi}_j \cos \phi_j - l_j \dot{\phi}_j^2 \sin \phi_j + l_j \ddot{\phi}_j \cos \phi_j, \\ & \ddot{l}_j \cos \phi_j \cos \theta_j - 2\dot{l}_j \dot{\phi}_j \sin \phi_j \cos \theta_j - 2\dot{l}_j \dot{\theta}_j \cos \phi_j \sin \theta_j - l_j \dot{\phi}_j^2 \cos \phi_j \cos \theta_j \\ & - l_j \ddot{\phi}_j \sin \phi_j \cos \theta_j + 2l_j \dot{\theta}_j \dot{\phi}_j \sin \phi_j \sin \theta_j - l_j \dot{\theta}_j^2 \cos \phi_j \cos \theta_j - l_j \ddot{\theta}_j \cos \phi_j \sin \theta_j] \end{aligned} \quad (6)$$

The components of acceleration in Eq. (6) are coupled to each other when expressed in the inertial frame, but are obviously decoupled from the surrounding masses. If we define a tether body frame which is attached to the tether with one axis tangent to the  $j$ th tether element, then the transformation between the inertial axes and the tether body frame is readily derived as

$$C_j^{B/I} = \begin{bmatrix} \cos \theta_j & 0 & -\sin \theta_j \\ -\sin \theta_j \sin \phi_j & \cos \phi_j & -\cos \theta_j \sin \phi_j \\ \cos \phi_j \sin \theta_j & \sin \phi_j & \cos \phi_j \cos \theta_j \end{bmatrix} \quad (7)$$

With this transformation, the acceleration terms in the body frame can be written as

$$\ddot{\mathbf{r}}_j^b = [l_j \ddot{\theta}_j \cos \phi_j + 2\dot{l}_j \dot{\theta}_j \cos \phi_j - 2l_j \dot{\theta}_j \dot{\phi}_j \sin \phi_j, l_j \ddot{\phi}_j + l_j \dot{\theta}_j^2 \sin \phi_j \cos \phi_j + 2\dot{l}_j \dot{\phi}_j, \ddot{l}_j - l_j \cos^2 \phi_j \dot{\theta}_j^2 - l_j \dot{\phi}_j^2] \quad (8)$$

A vector that is tangent to the  $j$ th element is given as the last row of the matrix in Eq. (7). Hence, the tension vector for the  $j$ th element can be written as

$$\mathbf{T}_j = T_j[\cos \phi_j \sin \theta_j, \sin \phi_j, \cos \phi_j \cos \theta_j] \quad (9)$$

Using this definition, the forces acting on the  $j$  th mass can be written as

$$\mathbf{F}_j = [F_{x_j}, F_{y_j}, F_{z_j}] + \mathbf{T}_{j-1} - \mathbf{T}_j \quad (10)$$

where  $[F_{x_j}, F_{y_j}, F_{z_j}]$  contain all external forces acting on the cable except the tension. After applying the coordinate transformation in Eq. (7) to the right hand side of Eq. (4), the right hand side of the equations of motion expressed in the tether body frame are obtained as

$$F_{\theta_j}^b = \frac{1}{m_j} (F_{x_j} \cos \theta_j - F_{z_j} \sin \theta_j + T_{j-1} \cos \theta_j \cos \phi_{j-1} \sin \theta_{j-1} - T_{j-1} \sin \theta_j \cos \phi_{j-1} \cos \theta_{j-1}) \\ + \frac{1}{m_{j+1}} (F_{z_{j+1}} \sin \theta_j - F_{x_{j+1}} \cos \theta_j + T_{j+1} \cos \theta_j \cos \phi_{j+1} \sin \theta_{j+1} - T_{j+1} \sin \theta_j \cos \phi_{j+1} \cos \theta_{j+1}) \quad (11)$$

$$F_{\phi_j}^b = \frac{1}{m_j} (-\sin \theta_j \sin \phi_j F_{x_j} - T_{j-1} \sin \theta_j \sin \phi_j \cos \phi_{j-1} \sin \theta_{j-1} + T_j \sin^2 \theta_j \sin \phi_j \cos \phi_j + F_{y_j} \cos \phi_j \\ + T_{j-1} \cos \phi_j \sin \phi_{j-1} - T_j \cos \phi_j \sin \phi_j - F_{z_j} \cos \theta_j \sin \phi_j - T_{j-1} \cos \theta_j \sin \phi_j \cos \phi_{j-1} \cos \theta_{j-1} \\ + T_j \cos^2 \theta_j \sin \phi_j \cos \phi_j) \quad (12)$$

$$+ \frac{1}{m_{j+1}} (F_{x_{j+1}} \sin \theta_j \sin \phi_j + T_j \sin^2 \theta_j \sin \phi_j \cos \phi_j - T_{j+1} \sin \theta_j \sin \phi_j \cos \phi_{j+1} \sin \theta_{j+1} - F_{y_{j+1}} \cos \phi_j \\ - T_j \cos \phi_j \sin \phi_j + T_{j+1} \cos \phi_j \sin \phi_{j+1} + F_{z_{j+1}} \cos \theta_j \sin \phi_j + T_j \cos^2 \theta_j \sin \phi_j \cos \phi_j \\ - T_{j+1} \cos \theta_j \sin \phi_j \cos \phi_{j+1} \cos \theta_{j+1})$$

$$F_{\psi_j}^b = \frac{1}{m_j} (\sin \theta_j \cos \phi_j F_{x_j} + T_{j-1} \sin \theta_j \cos \phi_j \cos \phi_{j-1} \sin \theta_{j-1} - T_j \sin^2 \theta_j \cos^2 \phi_j + F_{y_j} \sin \phi_j \\ + T_{j-1} \sin \phi_j \sin \phi_{j-1} - T_j \sin^2 \phi_j + F_{z_j} \cos \theta_j \cos \phi_j - T_{j-1} \cos \theta_j \cos \phi_j \cos \phi_{j-1} \cos \theta_{j-1} \\ - T_j \cos^2 \theta_j \cos^2 \phi_j) \quad (13)$$

$$+ \frac{1}{m_{j+1}} (-F_{x_{j+1}} \sin \theta_j \cos \phi_j - T_j \sin^2 \theta_j \cos^2 \phi_j + T_{j+1} \sin \theta_j \cos \phi_j \cos \phi_{j+1} \sin \theta_{j+1} - F_{y_{j+1}} \sin \phi_j$$

$$- T_j \sin^2 \phi_j + T_{j+1} \sin \phi_j \sin \phi_{j+1} - F_{z_{j+1}} \cos \theta_j \cos \phi_j + T_j \cos^2 \theta_j \cos^2 \phi_j \\ + T_{j+1} \cos \theta_j \cos \phi_j \cos \phi_{j+1} \cos \theta_{j+1})$$

The complete equations of motion must incorporate the relevant boundary conditions applicable to the real system. For example,  $T_{j-1} = 0$ ,  $\phi_{j-1} = 0$ ,  $\theta_{j-1} = 0$  for  $j = 1$ . In the following subsection the external forces on the cable are derived.

## A. External Tether Forces

The main forces acting on the tether system are aerodynamic drag, gravity, and forces from the kite. Each of these forces are dealt with in the following subsections.

### 1. Tether Drag

The drag forces acting on the tether are separated into normal and tangential components. First, the relative velocity of the wind is computed at the center of each segment according to

$$\mathbf{v}_j^c = \sum_{i=j+1}^n \dot{\mathbf{r}}_i + \dot{\mathbf{r}}_j / 2 - \mathbf{v}_j^w \quad (14)$$

where  $\mathbf{v}_j^w$  is the velocity vector of the wind components at the center of the  $j$ th cable element. The tangential component of the velocity along the cable segment is calculated by

$$\mathbf{v}_j^t = \left( \mathbf{v}_j^c \cdot \frac{\mathbf{r}_j}{|\mathbf{r}_j|} \right) \frac{\mathbf{r}_j}{|\mathbf{r}_j|} \quad (15)$$

The total drag force on the  $j$ th segment is then calculated by

$$\mathbf{F}_j^{d_c} = -\frac{1}{2} \rho C_D dl_j |\mathbf{v}_j|^2 \left( f_n \frac{\mathbf{v}_j^n}{|\mathbf{v}_j^n|} + f_t \frac{\mathbf{v}_j^t}{|\mathbf{v}_j^t|} \right) \quad (16)$$

where  $C_D$  is the cable drag coefficient, and  $f_n$  and  $f_t$  are the normal and tangential loading functions given by

$$f_n = 0.5 - 0.1 \cos \eta + 0.1 \sin \eta - 0.4 \cos 2\eta - 0.011 \sin 2\eta \quad (17)$$

$$f_t = 0.01 (2.008 - 0.3858\eta + 1.9159\eta^2 - 4.16147\eta^3 + 3.5064\eta^4 - 1.187299\eta^5) \quad (18)$$

where  $0 \leq \eta \leq \frac{\pi}{2}$  is the angle of attack, and  $\mathbf{v}_j^n \triangleq \mathbf{v}_j - \mathbf{v}_j^t$  is the component of the relative velocity normal to the cable segment, as shown in Fig. 3. In the lumped mass approximation, the drag forces from adjacent segments are lumped (or averaged) to the  $j$ th mass,

$$\mathbf{F}_j^{\text{drag}} := \begin{cases} (\mathbf{F}_j^{d_c} + \mathbf{F}_{j-1}^{d_c}) / 2, & j = n, \dots, 2 \\ \mathbf{F}_1^{d_c} / 2, & j = 1 \end{cases} \quad (19)$$

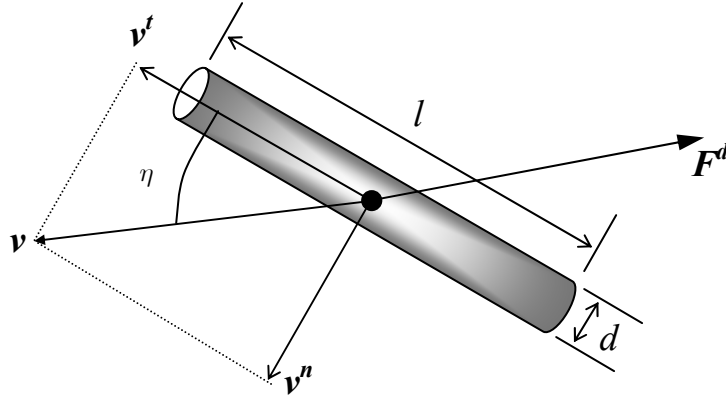


**Fig. 3 Representation of the components of drag on a cylinder.**

## 2. Gravity

The gravitational forces on the masses are applied using the mass distribution given in Eq. (1). In the inertial frame the force is defined as

$$\mathbf{F}_j^g = [0, 0, -m_j g] \quad (20)$$

### 3. Kite Lift and Drag

Probably the most important force acting on the tether is due to the kite. The lift and drag forces from the kite are applied directly at the end of the tether. The kite is assumed to be controlled by manipulating its angle of attack and roll angle. Thus, in this study, its attitude dynamics are ignored. This is the approach that was taken in Refs. 32 and 33, and is also the approach used for trajectory analysis for aircraft. A more detailed kite model is presented in Ref. 34. The incorporation of more representative kite models into the system model presented here is the subject of future research.

The lift and drag forces due to the kite are derived using a velocity coordinate system, as shown in Fig. 4.

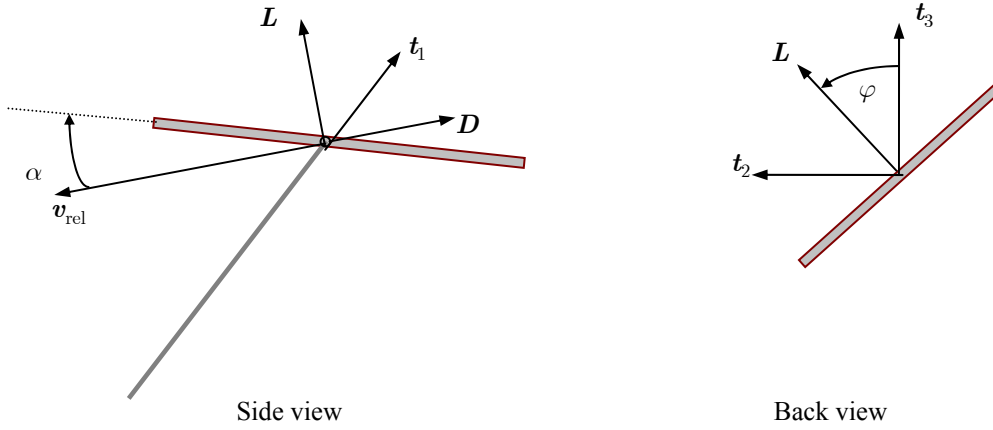


Fig. 4 Lift and drag forces on kite.

The vector that defines the plane containing the drag force and the velocity vector is given by

$$\mathbf{t}_2 = \frac{\mathbf{t}_1 \times \mathbf{v}_{\text{rel}}}{|\mathbf{t}_1 \times \mathbf{v}_{\text{rel}}|} \quad (21)$$

where  $\mathbf{t}_1 = [\sin \theta_1 \cos \phi_1, \sin \phi_1, \cos \theta_1 \cos \phi_1]$  is a vector tangential to the cable, and  $\mathbf{v}_{\text{rel}} = \mathbf{v}_1 - \mathbf{v}_w$  is the kite velocity relative to the wind. The lift force, when the velocity roll angle is zero, is parallel to the vector

$$\mathbf{t}_3 = \frac{\mathbf{v}_{\text{rel}} \times \mathbf{t}_2}{|\mathbf{v}_{\text{rel}} \times \mathbf{t}_2|} \quad (22)$$

Hence, the lift and drag force vectors are defined according to

$$\mathbf{L} = \frac{1}{2} \rho C_L S |\mathbf{v}_{\text{rel}}|^2 (\mathbf{t}_2 \sin \varphi + \mathbf{t}_3 \cos \varphi), \quad \mathbf{D} = -\frac{1}{2} \rho C_D S |\mathbf{v}_{\text{rel}}| \mathbf{v}_{\text{rel}} \quad (23)$$

It should be noted that the roll angle is defined here relative to the tether line. This is not the traditional roll angle, which is typically taken relative to an inertial axis system. The advantage of the definition used here is that it makes the roll angle independent of the local tether direction. This has implications for control implementation as the wind direction changes.

## B. Internal Tension Determination

Unfortunately, the equations of motion defined by Eqs. (8), and (11) through (13), together with the external forces, can not be solved immediately because the  $n$  tension forces appearing in Eqs. (11) through (13) are unknown. It should be noted, of course, that these forces could be calculated from the segment lengths and a constitutive law for the material, i.e., by inclusion of tether elasticity. In fact, the equations of motion as derived are quite general and can be applied in such a case. Therefore, the equations are written in a convenient reusable form if tether stretching needs to be included in the model. To integrate the system of equations, the fact that the segment lengths are known (they are either fixed, or the element closest to the deployer varies in length – see next section) is used to determine the tension forces.

Using knowledge of the tether lengths allows the third equation of motion in the tether body frame to be written as an algebraic equation. All variables appearing in the set of equations, including the right-hand side defined by Eq. (13), are known except the tension forces. The  $n$ -equations must be solved simultaneously for the  $n$  tension forces, which is achieved efficiently via a Gaussian elimination algorithm (LAPACK is used for the implementation of this algorithm). Note that this is much more efficient than typical implementations using Cartesian coordinates that require constraint stabilization and the differentiation of the constraint equations, i.e., only the angular generalized coordinates need to be integrated here. Once the tensions are determined, they are substituted into the remaining equations of motion for integration.

## C. Incorporating a Variable Length Tether

The tether is modeled as a collection of lumped masses connected by inelastic links, which makes dealing with the case of a variable length tether difficult. In particular, it is necessary to have a state vector of variable dimension and to add and subtract elements from the model at appropriate times. When the tether is treated as elastic, great care needs to be exercised to ensure that the introduction of new elements does not create unnecessary cable oscillations. This can happen if the position of the new mass results in the incorrect tension in the new element. However, for an inelastic tether, the introduction of a new mass occurs such that it is placed along the same line as the existing element. Thus, the new initial conditions for the incoming element are that it has the same angles and angle rates as the existing element (closest to the deployer). If the critical length for introduction of a new element is defined as  $l^* \triangleq (1 + k^*)l_{\text{nom}}$ , then the new element is initialized with a length of  $k^*$  in nondimensional units, and the same length rate as the previous  $n$ th element. This process is illustrated in Fig. 5a.

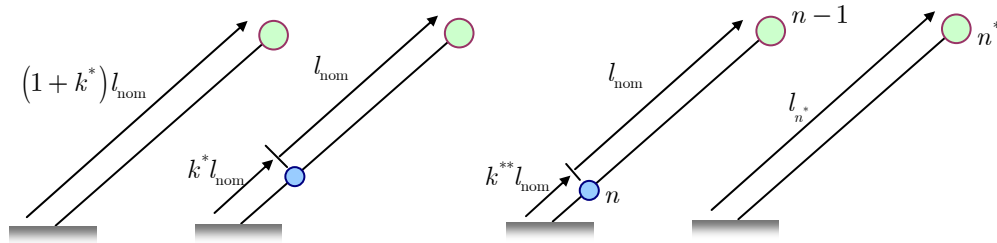


**Fig. 5 a) Addition of elements to cable model during deployment, b) removal of element during retrieval.**

During retrieval, elements must be removed. Here, the  $n$ th element to be removed and the  $(n-1)$ th element needs to be used to update the initial conditions for the new  $n^*$ th element. In this work, the position and velocity of the  $(n-1)$ th mass is used to initialize the  $n^*$ th element. In order for the dynamics of the system to remain as continuous as possible, it is important that the positions and velocities of all remaining elements are unaltered by the removal of an element. Thus, let

$$\begin{aligned}
 x_{n-1} &= l_n \sin \theta_n \cos \phi_n + l_{n-1} \sin \theta_{n-1} \cos \phi_{n-1} \\
 y_{n-1} &= l_n \sin \phi_n + l_{n-1} \sin \phi_{n-1} \\
 z_{n-1} &= l_n \cos \theta_n \cos \phi_n + l_{n-1} \cos \theta_{n-1} \cos \phi_{n-1}
 \end{aligned} \tag{24}$$

From which

$$\begin{aligned}
l_n^* &= \sqrt{x_{n-1}^2 + y_{n-1}^2 + z_{n-1}^2} \\
\theta_n^* &= \text{atan2}(x_{n-1}, z_{n-1}) \\
\phi_n^* &= \sin^{-1}(y_{n-1}/l_n^*)
\end{aligned} \tag{25}$$

Similarly, the relative velocity of the  $(n-1)$ th mass in the inertial frame is given by

$$\begin{aligned}
\dot{x}_{n-1} &= \dot{l}_n \sin \theta_n \cos \phi_n + l_n \dot{\theta}_n \cos \theta_n \cos \phi_n - l_n \dot{\phi}_n \sin \theta_n \sin \phi_n \\
&\quad + \dot{l}_{n-1} \sin \theta_{n-1} \cos \phi_{n-1} + l_{n-1} \dot{\theta}_{n-1} \cos \theta_{n-1} \cos \phi_{n-1} - l_{n-1} \dot{\phi}_{n-1} \sin \theta_{n-1} \sin \phi_{n-1} \\
\dot{y}_{n-1} &= \dot{l}_n \sin \phi_n + l_n \dot{\phi}_n \cos \phi_n + \dot{l}_{n-1} \sin \phi_{n-1} + l_{n-1} \dot{\phi}_{n-1} \cos \phi_{n-1} \\
\dot{z}_{n-1} &= \dot{l}_n \cos \theta_n \cos \phi_n - l_n \dot{\theta}_n \sin \theta_n \cos \phi_n - l_n \dot{\phi}_n \cos \theta_n \sin \phi_n \\
&\quad + \dot{l}_{n-1} \cos \theta_{n-1} \cos \phi_{n-1} - l_{n-1} \dot{\theta}_{n-1} \sin \theta_{n-1} \cos \phi_{n-1} - l_{n-1} \dot{\phi}_{n-1} \cos \theta_{n-1} \sin \phi_{n-1}
\end{aligned} \tag{26}$$

From which

$$\begin{aligned}
\dot{l}_n^* &= \dot{x}_{n-1} \cos \phi_n^* \sin \theta_n^* + \dot{y}_{n-1} \sin \phi_n^* + \dot{z}_{n-1} \cos \phi_n^* \cos \theta_n^* \\
\dot{\theta}_n^* &= (\dot{x}_{n-1} \cos \theta_n^* - \dot{z}_{n-1} \sin \theta_n^*) / (l_n^* \cos \phi_n^*) \\
\dot{\phi}_n^* &= (\dot{y}_{n-1} \cos \phi_n^* - \dot{z}_{n-1} \sin \phi_n^* \cos \theta_n^* - \dot{x}_{n-1} \sin \phi_n^* \sin \theta_n^*) / l_n^*
\end{aligned} \tag{27}$$

It should be noted that these updates keep the position and velocity of the  $(n-1)$ th mass the same across the update. The reason for this is that the positions and velocities of all subsequent masses depend on the position/velocity of the  $n$ th mass. Hence, if this is changed, then the position and velocity of all masses representing the tether change instantaneously. The accuracy of the updates depend on the transition parameter  $k^{**}$ , which is used to monitor the length of the  $n$ th segment. An element is removed when  $l_n < k^{**} l_{\text{nom}}$ . Because the tether is inelastic, altering the length of the new  $n$ th element does not keep the total tether length or mass constant unless the  $n$ th and  $(n-1)$ th elements are tangential. Therefore, by choosing  $k^{**}$  small enough, the errors in the approximation can be made small.

### III. Kite and Tether Feedback Control

The issue of stabilizing and controlling a flexible kite is a complex one. As yet, suitable kite models applicable to flight control design have not been fully realized. Hence, we proceed with a point mass kite model, assuming that the angle of attack and roll angle are control variables. This implies that the magnitude and direction of lift are controlled/demanded, rather than actual actuator deflections. In Ref. 34, it was demonstrated that control of the kite motion can be achieved by moving the positions of the attachment points on the kite wingtips. However, this requires a more complex model of the kite. The goal of future inner-loop design for the kite will be to move the tether attachment points to achieve a demanded angle of attack and roll angle.

In addition to control of the kite itself, the tether length is also a control input into the system. The ultimate objective of the tethered kite system is to generate power, as discussed elsewhere.<sup>33</sup> In this paper, we present basic controllers to manipulate the motion of the kite system. The key variables to consider are: 1) kite altitude, 2) kite cross-wind position, 3) tether tension. In this study, we are not interested in the downwind position of the kite.

The key variables considered for control of the kite motion are shown in Fig. 6. Effectively, the kite altitude can be controlled by the amount of tether deployed, provided that the kite is generating sufficient lift. The amount of lift generated by the kite controls the tension in the line. Therefore, the angle of attack is used to regulate the tether tension. The cross-wind position of the kite can be controlled by the roll angle. However, all three outputs are

influenced by all three inputs. For example, increasing the angle of attack results in larger lift forces, which tends to make the tether more vertical. There is a limit, however, before the induced drag is enough to offset the gain in altitude. The predominant altitude of the kite for a steady value of lift is dominated by the amount of deployed tether.

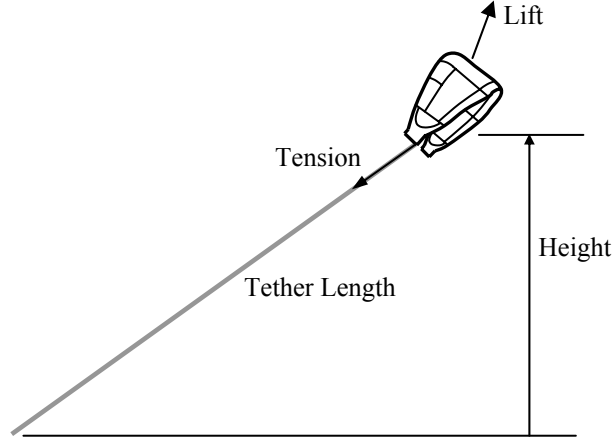


**Fig. 6 Key variables for kite control.**

The tether length is controlled via the second derivative of the tether length using the following feedback law

$$\ddot{L}_c = k_{\ddot{L}} (\dot{L}_c - \dot{L}) \quad (28)$$

$$\ddot{L} = \begin{cases} \ddot{L}_{\min} & \ddot{L}_c \leq \ddot{L}_{\min} \\ \ddot{L}_c & \ddot{L}_{\min} < \ddot{L}_c < \ddot{L}_{\max} \\ \ddot{L}_{\max} & \ddot{L}_c \geq \ddot{L}_{\max} \end{cases} \quad (29)$$

$$\dot{L}_c = k_{\dot{L}} (h_c - h_{\text{kite}}) \quad (30)$$

$$\dot{L} = \begin{cases} \dot{L}_{\min} & \dot{L}_c \leq \dot{L}_{\min} \\ \dot{L}_c & \dot{L}_{\min} < \dot{L}_c < \dot{L}_{\max} \\ \dot{L}_{\max} & \dot{L}_c \geq \dot{L}_{\max} \end{cases} \quad (31)$$

The use of the length acceleration rather than purely length rate is due to the fact that the model uses the equation of motion for the tether segment lengths to compute the tether tension. When the tether is modeled as elastic, the tether length is not restricted to being controlled through the acceleration. However, control via acceleration tends to make the deployment smoother. A commanded altitude is input,  $h_c$ . The measured altitude of the kite,  $h_{\text{kite}}$ , is used to produce a proportional command for the tether length rate. The length rate command is subject to saturation limits given by Eq. (31). The commanded length rate is compared to the measured length rate. The error is used to produce a proportional demand for the tether length acceleration. The length acceleration is also subject to saturation limits.

The kite roll angle is used to control the direction of the lift vector. A commanded roll angle is specified by the following expression

$$\varphi_c = \sin^{-1} \left( \frac{\int k_y (y_c - y_{\text{kite}}) dt + k_y \dot{y}_{\text{kite}} - k_y^1 p_1}{v_{\text{rel}}^x \cos \phi_1 \cos \theta_1 - v_{\text{rel}}^z \cos \phi_1 \sin \theta_1} \right) \quad (32)$$

where

$$p_1 = v_{\text{rel}}^z (v_{\text{rel}}^z \sin \phi_1 - v_{\text{rel}}^y \cos \phi_1 \cos \theta_1) - v_{\text{rel}}^x (v_{\text{rel}}^y \cos \phi_1 \sin \theta_1 - v_{\text{rel}}^x \sin \phi_1) \quad (33)$$

This roll angle is derived based on the definition of the direction of the lift vector at the end of the tether. It uses the commanded position of the kite,  $y_c$ , and feedback of the measured cross-wind position  $y_{\text{kite}}$  and the cross-wind kite velocity. The cross-wind kite velocity is used to provide damping of the motion. The error in cross-wind position is integrated to account for the fact that the desired roll angle is not linearly proportional to the cross-wind error.

The actual roll is limited by the following saturation limits

$$\varphi = \begin{cases} \varphi_{\min} & \varphi_c \leq \varphi_{\min} \\ \varphi_c & \varphi_{\min} < \varphi_c < \varphi_{\max} \\ \varphi_{\max} & \varphi_c \geq \varphi_{\max} \end{cases} \quad (34)$$

This also implies that the integral in Eq. (32) is subject to antiwindup protection. The implementation of Eq. (34) is also subject to a slew rate limit to prevent instantaneous changes in roll angle.

The kite lift is controlled via the angle of attack. The rate of angle of attack is commanded as follows

$$\dot{\bar{\alpha}}_c = k_{\alpha} (T_c - T_{k-1} \cos \theta_1 \cos \phi_1) \quad (35)$$

where  $T_c$  is the commanded tether tension. It is important to point out that the commanded tether tension is actually the component of tension in the vertical direction. Therefore, the feedback ensures that the kite keeps the tether as vertical as possible. The actual angle of attack rate is limited by

$$\dot{\bar{\alpha}} = \begin{cases} \dot{\bar{\alpha}}_{\min} & \dot{\bar{\alpha}}_c \leq \dot{\bar{\alpha}}_{\min} \\ \dot{\bar{\alpha}}_c & \dot{\bar{\alpha}}_{\min} < \dot{\bar{\alpha}}_c < \dot{\bar{\alpha}}_{\max} \\ \dot{\bar{\alpha}}_{\max} & \dot{\bar{\alpha}}_c \geq \dot{\bar{\alpha}}_{\max} \end{cases} \quad (36)$$

The actual angle of attack is implemented as a function of the integral of Eq. (36) as

$$\alpha = \frac{\bar{\alpha}}{p_2 \sin \varphi + p_3 \cos \varphi} \quad (37)$$

where

$$p_2 = \frac{v_{\text{rel}}^y \cos \phi_1 \sin \theta_1 - v_{\text{rel}}^x \sin \phi_1}{|\mathbf{t}_1 \times \mathbf{v}_{\text{rel}}|} \quad (38)$$

$$p_3 = \frac{v_{\text{rel}}^x (v_{\text{rel}}^x \cos \phi_1 \cos \theta_1 - v_{\text{rel}}^z \cos \phi_1 \sin \theta_1) - v_{\text{rel}}^y (v_{\text{rel}}^z \sin \phi_1 - v_{\text{rel}}^y \cos \phi_1 \cos \theta_1)}{|\mathbf{v}_{\text{rel}} \times (\mathbf{t}_1 \times \mathbf{v}_{\text{rel}})|} \quad (39)$$

$$t_1 = r_1 / |r_1| \quad (40)$$

Note that the angles used in Eqs. (38) and (39) represent the tangential direction of the tether at the kite. We note that the requirements for these feedback laws are the kite position, cross-wind velocity, tether length and length rate, tension vector at the kite, and relative wind speed at the kite.

#### IV. Numerical Results

To illustrate the combined interaction of the tether model and the feedback controllers, we consider the scenario where we would like the kite to reach an altitude of 3200 m, and move across the wind in a sinusoidal pattern with a frequency of  $2\pi/20$  Hz, with the tether tension maintained at 900 N. The kite has an area of 25 m<sup>2</sup>, a mass of 20 kg, the tether length is initially 3000 m, the tether mass density is 1000 kg/m<sup>3</sup>, the drag coefficient is 1.2, and the diameter is 1 mm. The nominal wind profile is given by  $W_x = 15 - 15\exp(-h/500)$  m/s. The feedback control gains were selected as:  $k_h = 0.03$ ,  $k_{\dot{L}} = 1$ ,  $k_y = 0.1$ ,  $\dot{L}_{\max} = 5$  m/s,  $\ddot{L}_{\max} = 1$  m/s<sup>2</sup>,  $k_\alpha = 0.001$ ,  $k_\phi = 0.1$ ,  $\alpha_{\max} = 15$  deg,  $\dot{\phi}_{\max} = 20$  deg/sec,  $\dot{\alpha}_{\max} = 5$  deg/sec. The kite aerodynamic coefficients are assumed to be  $C_{D_0} = 0.02$ ,  $k = 0.1$ ,  $C_{L_\alpha} = 4.4$  /rad. Simulation results are shown in Fig. 7 through Fig. 12 for the case of a steady wind (thick green line), together with the results from 20 Monte Carlo simulations wind random wind gusts. The random winds are limited to a maximum of 1 m/s in-plane and 2 m/s in the cross-wind direction. The cable is modeled using 200 m long segments.

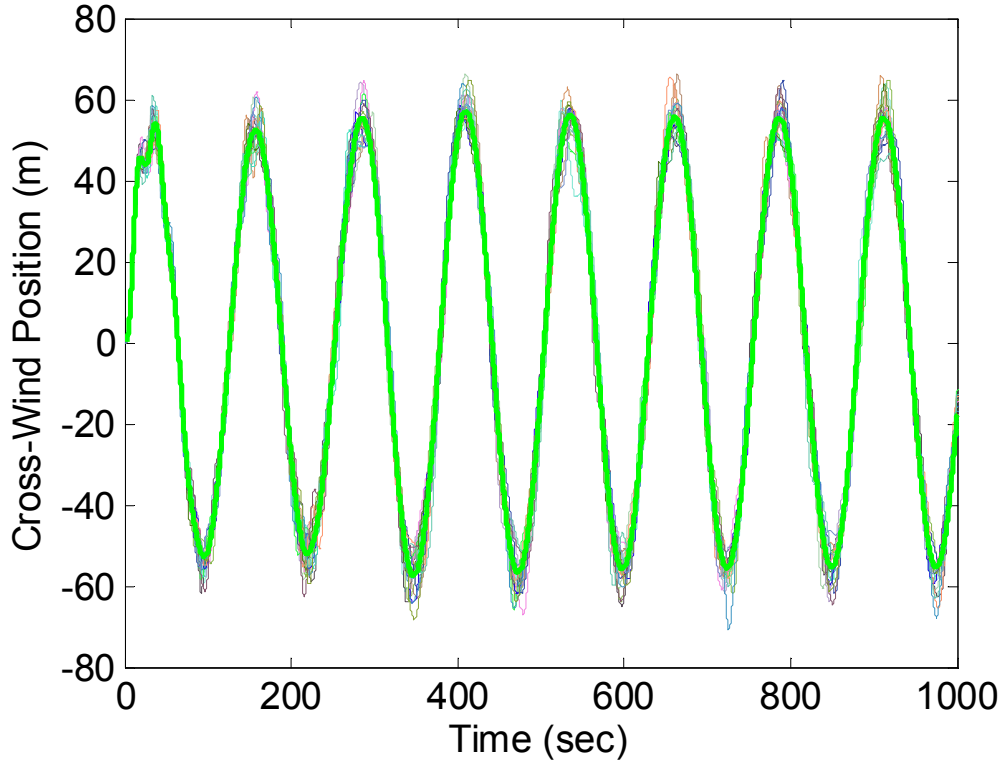


Fig. 7 Kite cross-wind position.

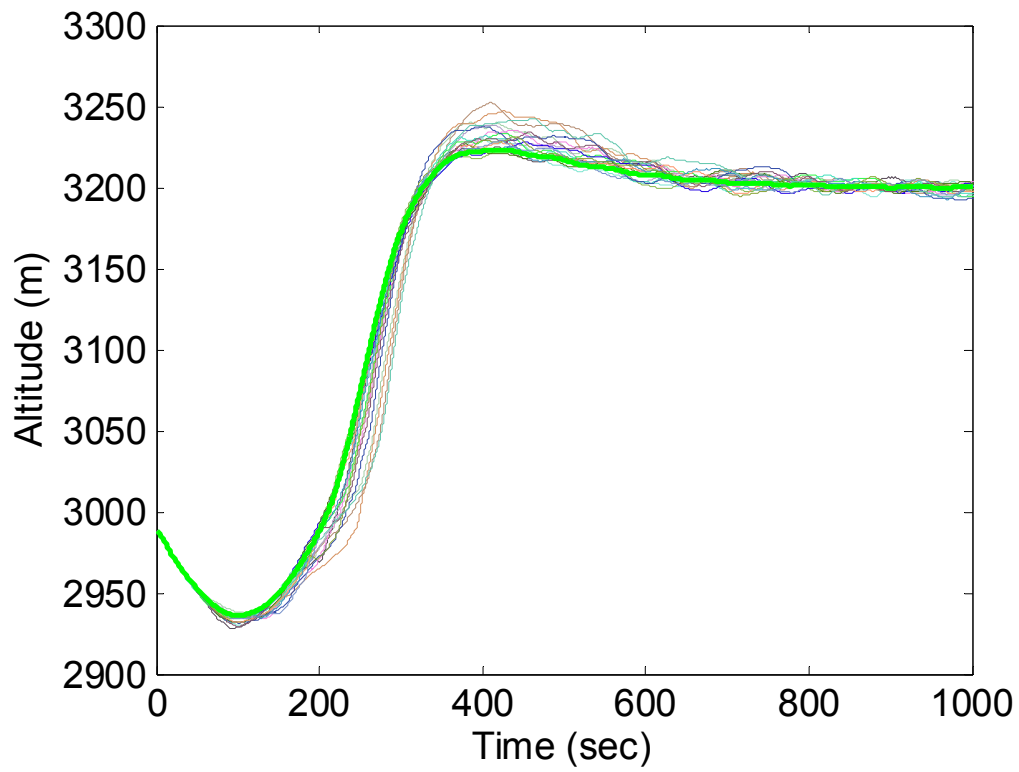


Fig. 8 Kite altitude.

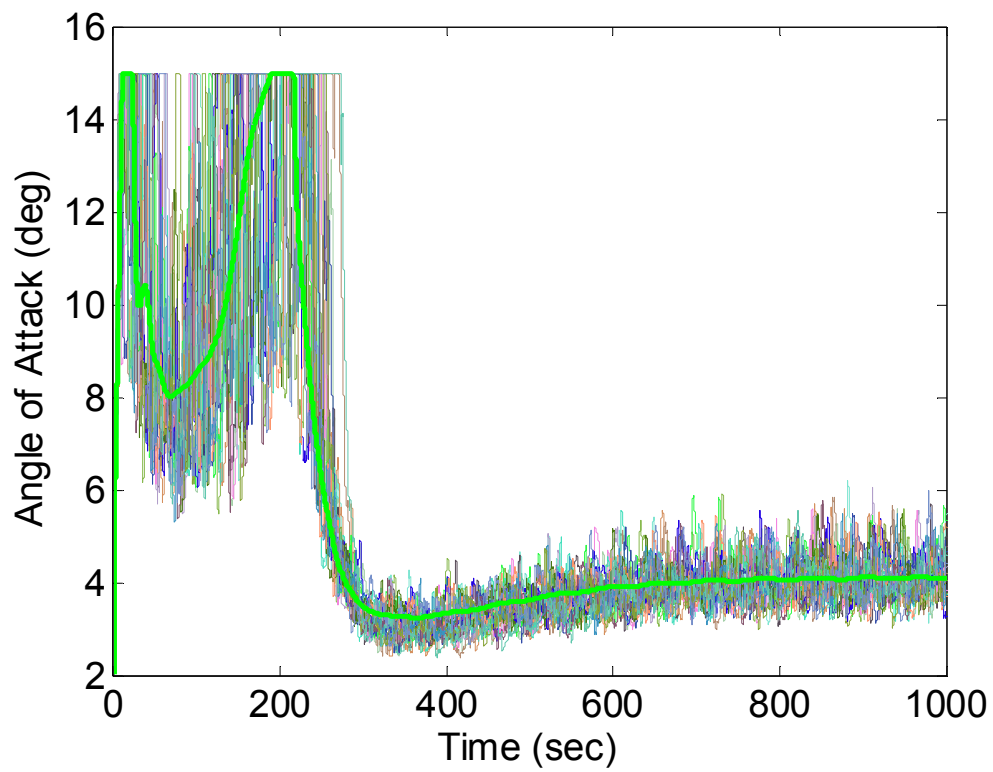


Fig. 9 Kite angle of attack.

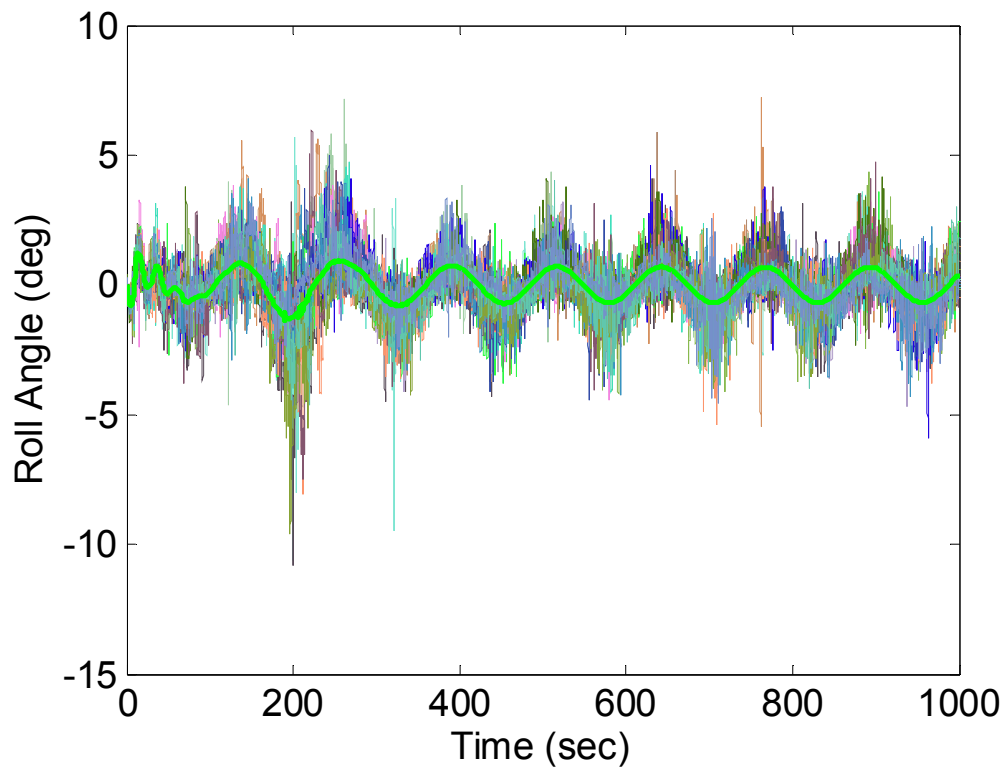


Fig. 10 Kite roll angle.

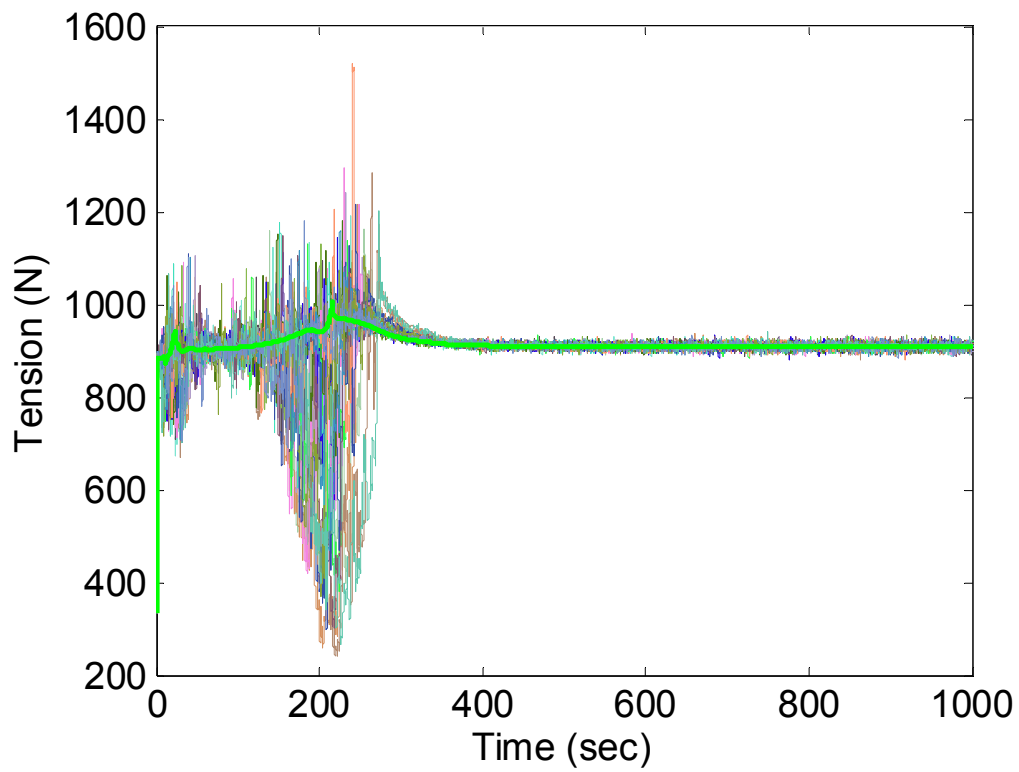
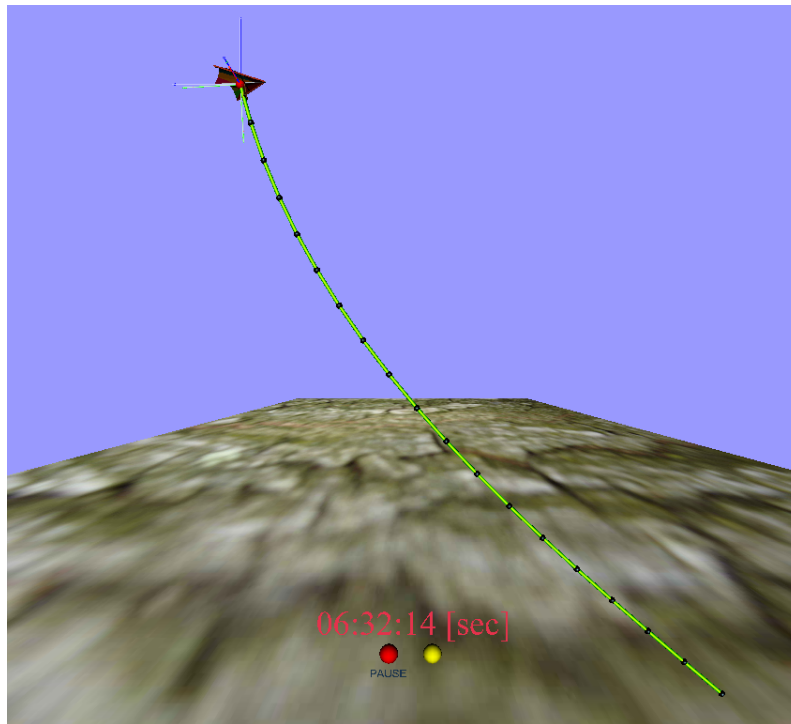


Fig. 11 Tether tension.



**Fig. 12 Tether shape during simulation.**

Fig. 7 shows the cross-wind position of the kite. On the scale of plot it can be seen that there is very little difference between the different simulation cases. In the nominal case, the kite positions follows the desired path very well, with approximately 5 m error at the extremes of the sine wave. The random winds affect the tracking error predominantly at the extremes of the trajectory due to the fact that the kite is moving at its slowest relative speed at these points. Fig. 8 shows that the kite is initially about 200 m below the desired altitude. The initial configuration of the system is nearly vertical, which is significantly out of equilibrium for the applied winds. Hence, the kite initially drops in altitude as it is taken downwind. The tether is reeled out simultaneously, until the desired altitude is eventually reached. In the unsteady winds, the kite follows the same basic pattern, with slightly different overshoots in altitude. The kite altitude is controlled reasonably well. There are no sudden drops in altitude, and the error relative to the constant winds case is on the order of about 10 m. Fig. 9 shows the kite angle of attack, Fig. 10 shows the roll angle, and Fig. 11 shows the tether tension. It can be seen in the steady wind case that the control inputs are very smooth, with all states converging very close to the desired values. The angle of attack saturates at the maximum allowable of 15 deg near the beginning of the simulation, but settles down to a nearly constant value for steady winds. The unsteady winds have a significant effect on the required angle of attack to achieve the desired tension at the kite. This is due to the fluctuations in tether tension as the winds change. In practice, the real tension would not be expected to change so rapidly due to the delays caused by the tether elasticity. Furthermore, internal damping in the tether would also prevent large spikes in the tension. The measured tension would be similarly noisy. However, the measured tension would not be fed back directly. Instead, it would be filtered to remove the high frequency content and noise. Hence, one might expected the angle of attack to converge more towards the steady wind case. The roll angle of the kite varies very moderately in the case of a steady wind. The peak to peak amplitude is on the order of 0.7 deg. In the case of unsteady winds, peaks of up to 10 deg are observed. Fig. 12 shows an example of the tether shape taken from an animation of the simulation results. It is evident that the tether does not maintain a straight line shape.

Consider now the case where it is desired to deploy the kite a significant distance. The kite is initially attached to a 300 m long tether, and the desired final altitude is 2000 m. Deployment is commanded after 100 sec using a cosine variation in altitude. Simulations were performed with the model using segment lengths of 100 m. Furthermore, both steady and unsteady winds were considered. In the case of unsteady winds, only cross-wind

components are considered. The same parameters and gains are used as in the previous case. Numerical results are shown in Fig. 13 through Fig. 18. Fig. 13 shows the cross-wind component of the kite position during deployment. The results show that the cross-wind error is kept within a mean of approximately 5 m. The results also show that the mean error tends to increase throughout the simulation. This is the result of the increase in tether length. Fig. 14 shows the kite altitude throughout the deployment. The effect of the cross-winds on altitude is negligible compared with the true altitude of the kite. It can be seen that the kite follows the cosine-deployment quite well with minimal overshoot. Fig. 15 shows the kite angle of attack, which is initially saturated due to the combination of low wind speed at 300 m altitude, and the lack of tension in the tether. When the tether starts deploying, and the tension begins to increase, the angle of attack reduces. The variation in angle of attack is very smooth, even in the case of cross-wind disturbances. Fig. 16 shows that the majority of the unsteady winds are compensated for by changes in the kite roll angle. Peak roll angles on the order of about 2 deg are required. Fig. 17 shows that the tether tension is initially quite low. This is caused by the initial angle of attack, which is set to 2 deg. For a tether length of 300 m and the specified winds, the maximum tension that can be induced is about 600 N. When the kite reaches higher altitudes, the tension increases until it eventually converges to the desired value of 900 N. Finally, Fig. 18 shows the unsteady wind that is applied during the simulation. It is interesting to note that the mean cross-wind (y) error remains approximately zero despite the change in the wind direction. Fig. 16 shows that this is achieved via a mean change in the kite roll angle.

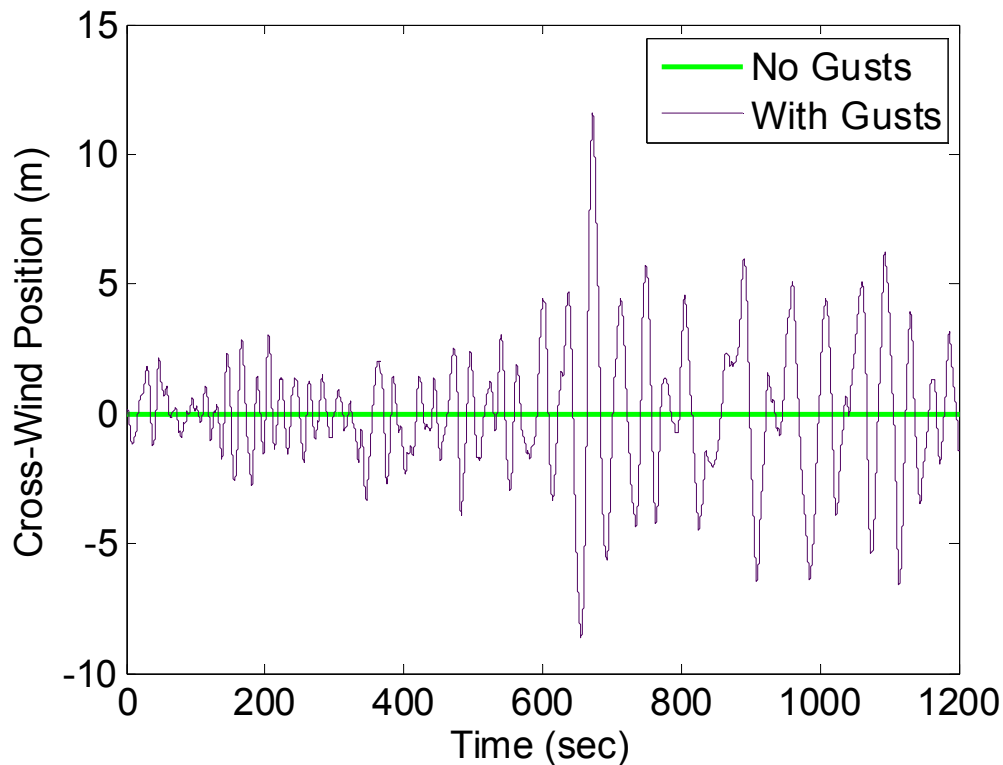


**Fig. 13** Cross-wind position of kite during deployment to 2 km altitude.

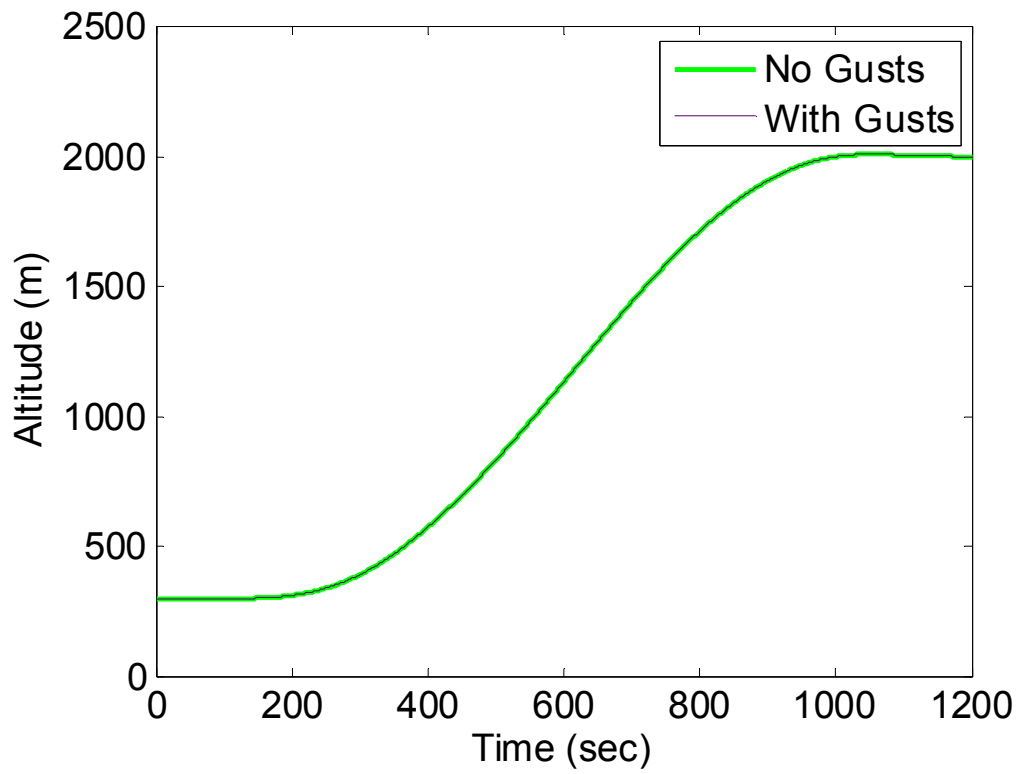


Fig. 14 Kite altitude during deployment.

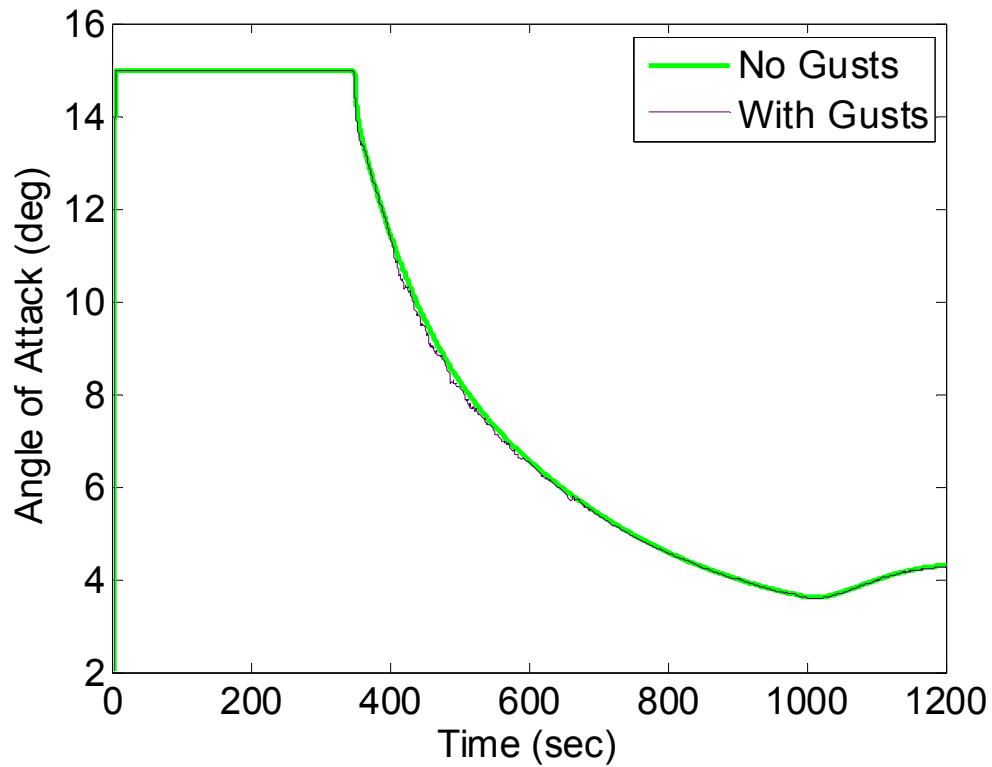


Fig. 15 Kite angle of attack during deployment.

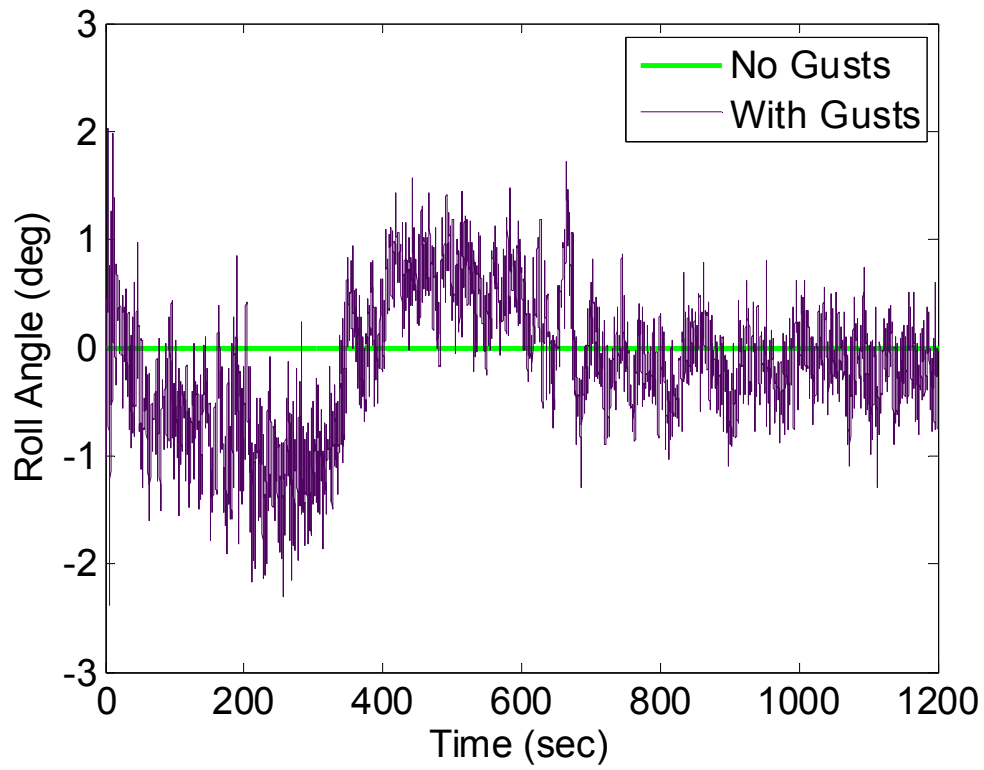


Fig. 16 Roll angle of kite during deployment.

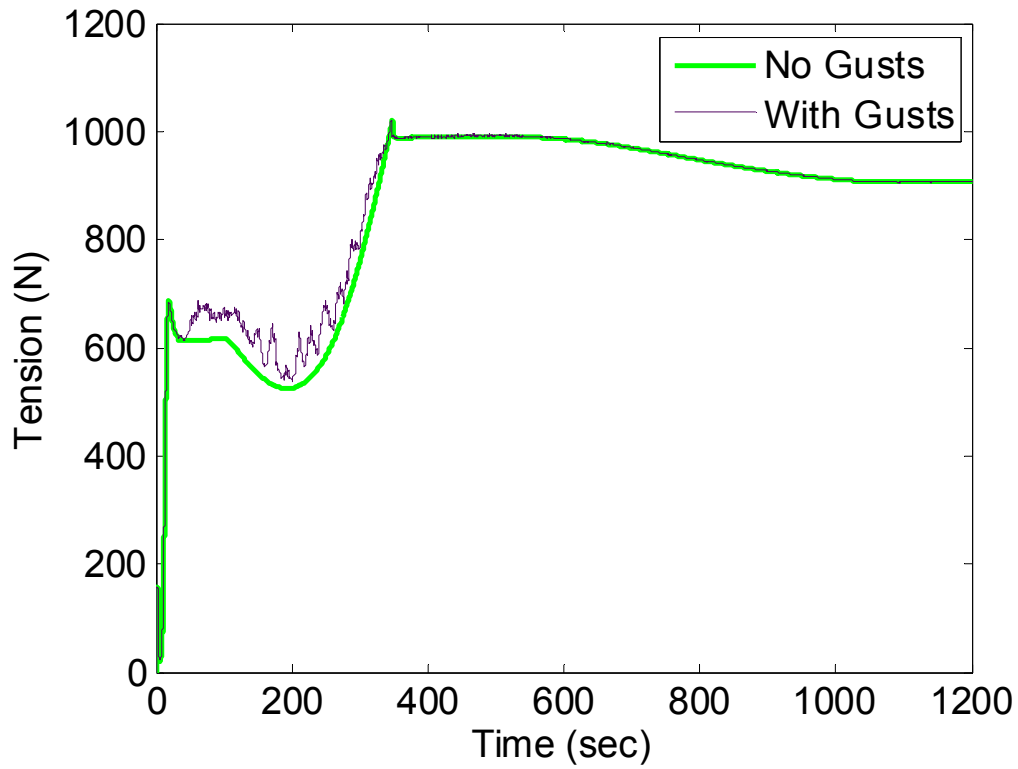
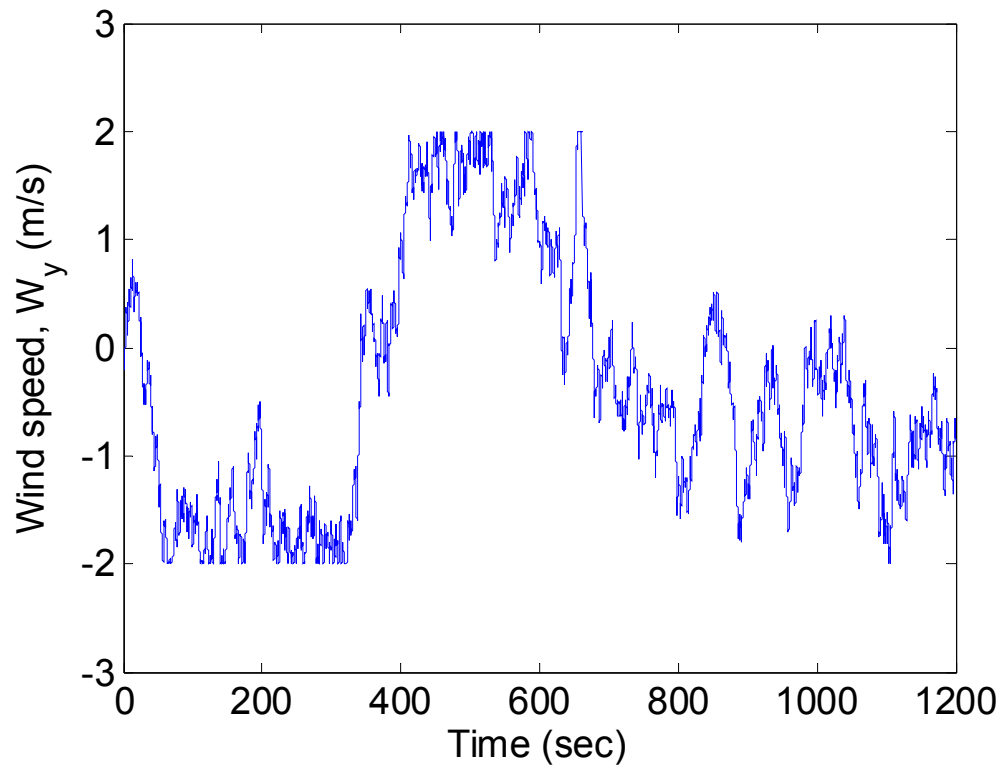


Fig. 17 Tether tension during kite deployment.



**Fig. 18 Example of cross-wind component of wind during deployment.**

### Conclusions

A dynamic model of a tethered kite system has been derived based on a lumped mass methodology. The model is able to simulate the dynamics of a variable length tether by the addition and subtraction of elements. The cable is treated as inelastic to enable larger time steps to be taken than can be achieved using elastic cable models. Feedback controllers for the kite angle of attack, roll angle, and tether length were derived to manipulate the altitude, cross-wind position, and tether tension. Numerical simulations with steady and unsteady winds show that the kite can be successfully controlled to maintain altitude and tension, as well as fly a specified cross-wind trajectory.

### References

- <sup>1</sup>Carpenter, H.G., "Tethered Aircraft Having Remotely Controlled Angle of Attack," US Patent 5,931,416.
- <sup>2</sup>Carpenter, H.G., "Tethered Aircraft System for Gathering Energy From Wind," US Patent 6,254,034.
- <sup>3</sup>Roberts, B.W., and Shepard, D.H., "Unmanned Rotorcraft to Generate Electricity using Upper Atmospheric Winds," *Australian International Aerospace Congress*, Brisbane, July 2003.
- <sup>4</sup>Manalis, M.S., "Airborne Windmills: Energy Source for Communication Aerostats," AIAA Lighter Than Air Technology Conference, AIAA Paper 75-923, July 1975.
- <sup>5</sup>Manalis, M.S., "Airborne Windmills and Communication Aerostats," *Journal of Aircraft*, Vol. 13, No. 7, 1976, pp.543-544.
- <sup>6</sup>Riegler, G., and Riedler, W., "Tethered Wind Systems for the Generation of Electricity," *Journal of Solar Energy Engineering*, Vol. 106, 1984, pp.177-181.
- <sup>7</sup>Riegler, G., Riedler, W., and Horvath, E., "Transformation of Wind Energy by a High-Altitude Power Plant," *Journal of Energy*, Vol. 7, No. 1, 1983, pp.92-94.
- <sup>8</sup>Fletcher, C.A.J., and Roberts, B.W., "Electricity Generation from Jet-Stream Winds," *Journal of Energy*, Vol. 3, 1979, pp.241-249.

- <sup>9</sup> Fletcher, C.A.J., "On the Rotary Wing Concept for Jet Stream Electricity Generation," *Journal of Energy*, Vol. 7, No. 1, 1983, pp.90-92.
- <sup>10</sup> Rye, D.C., "Longitudinal Stability of a Hovering, Tethered Rotorcraft," *Journal of Guidance, Control, and Dynamics*, Vol. 8, No. 6, 1985, pp.743-752.
- <sup>11</sup> Fry, C.M., and Hise, H.W., "Wind Driven, High Altitude Power Apparatus," US Patent 4,084,102, April 1978.
- <sup>12</sup> Kling, A., "Wind Driven Power Plant," US Patent 4,073,516, Feb. 1978.
- <sup>13</sup> Pugh, P.F., "Wind Generator Kite System," US Patent 4,486,669, Dec. 1984.
- <sup>14</sup> Biscoomb, L.I., "Multiple Wind Turbine Tethered Airfoil Wind Energy Conversion System," US Patent 4,285,481, Aug. 1981.
- <sup>15</sup> Watson, W.K., "Airship-Floated Wind Turbine," US Patent 4,491,739, Jan. 1985.
- <sup>16</sup> Shepard, D.H., "Power Generation from High Altitude Winds," US Patent 4,659,940, April 1987.
- <sup>17</sup> Rundle, C.V., "Tethered Rotary Kite," US Patent 5,149,020, Sept. 1992.
- <sup>18</sup> Roberts, B.W., "Windmill Kite," US Patent 6,781,254, Aug. 2004.
- <sup>19</sup> Mouton, W.J., and Thompson, D.F., "Airship Power Turbine," US Patent 4,166,596, Sept. 1979.
- <sup>20</sup> Ockels, W.J., "Laddermill, a Novel Concept to Exploit the Energy in the Airspace," *Aircraft Design*, Vol. 4, 2001, pp.81-97.
- <sup>21</sup> Meijaard, J.P., Ockels, W.J., and Schwab, A.L., "Modelling of the Dynamic Behaviour of a Laddermill, A Novel Concept to Exploit Wind Energy," Proceedings of the Third International Symposium on Cable Dynamics, Norway, Aug. 1999, pp.229-234.
- <sup>22</sup> Lansdorp, B., and Ockels, W.J., "Comparison of Concepts for High-Altitude Wind Energy Generation with Ground Based Generator," Proceedings of the NRE 2005 Conference, Beijing, China, pp.409-417.
- <sup>23</sup> Lansdorp, B., Remes, B., and Ockels, W.J., "Design and Testing of a Remotely Controlled Surfkite for the Laddermill," World Wind Energy Conference, Melbourne, Australia, Nov. 2005.
- <sup>24</sup> Lansdorp, B., and Williams, P., "The Laddermill - Innovative Wind Energy from High Altitudes in Holland and Australia," Paper presented at Wind Power 2006, Adelaide, Australia, September 2006.
- <sup>25</sup> Bolonkin, A., "Utilization of Wind Energy at High Altitude," AIAA Paper 2004-5705, Aug. 2004.
- <sup>26</sup> Loyd, M.L., "Crosswind Kite Power," *Journal of Energy*, Vol. 4, No. 3, 1980, pp.106-111.
- <sup>27</sup> Varma, S.K., and Goela, J.S., "Effect of Wind Loading on the Design of a Kite Tether," *Journal of Energy*, Vol. 6, No. 5, 1982, pp.342-343.
- <sup>28</sup> Jackson, P.S., "Optimum Loading of a Tension Kite," *AIAA Journal*, Vol. 43, No. 11, 2005, pp.2273-2278.
- <sup>29</sup> Payne, P.R., and McCutchen, C., "Self-Erecting Windmill," US Patent 3,987,987, Oct. 1976.
- <sup>30</sup> Loeb, A., "Wind Driven Energy System," US Patent 4,124,182, Nov. 1978.
- <sup>31</sup> Lois, L., "Apparatus for Extracting Energy from Winds at Significant Height Above the Surface," US Patent 4,076,190, Feb. 1978.
- <sup>32</sup> Williams, P., "Optimal Wind Power Extraction with a Tethered Kite," AIAA Guidance, Navigation, and Control Conference, Keystone, Colorado, 21-24 August 2006, AIAA Paper 2006-6193.
- <sup>33</sup> Williams, P., Lansdorp, B., and Ockels, W., "Optimal Cross-Wind Towing and Power Generation with Tethered Kites," AIAA Guidance, Navigation and Control Conference, Aug. 2007.
- <sup>34</sup> Williams, P., Lansdorp, B., and Ockels, W., "Flexible Tethered Kite with Moveable Attachment Points I: Dynamics and Control," AIAA Atmospheric Flight Mechanics Conference, Aug. 2007.
- <sup>35</sup> Williams, P., Lansdorp, B., and Ockels, W., "Flexible Tethered Kite with Moveable Attachment Points II: State and Wind Estimation," AIAA Atmospheric Flight Mechanics Conference, Aug. 2007.
- <sup>36</sup> Williams, P., "Deployment/Retrieval Optimization for Flexible Tethered Satellite Systems," *Nonlinear Dynamics*, 2007.